NeuroImage 57 (2011) 1131–1139

Contents lists available at ScienceDirect

NeuroImage

journal homepage: www.elsevier.com/locate/ynimg

Inhibition in early Alzheimer's disease: An fMRI-based study of effective connectivity

Romana Rytsar [a], Eleonora Fornari [b], Richard S. Frackowiak [a], Joseph A. Ghika [a], Maria G. Knyazeva [a,c,*]

[a] Department of Clinical Neuroscience, Centre Hospitalier Universitaire Vaudois (CHUV), and University of Lausanne, Lausanne, Switzerland
[b] CIBM (Centre d'Imagérie Biomédicale), CHUV unit, Lausanne, Switzerland
[c] Department of Radiology, Centre Hospitalier Universitaire Vaudois (CHUV), and University of Lausanne, Lausanne, Switzerland

ARTICLE INFO

Article history:
Received 8 February 2011
Revised 11 April 2011
Accepted 9 May 2011
Available online 15 May 2011

Keywords:
Neurodegenerative mechanisms
Visual cortex
Neural plasticity
Functional magnetic resonance imaging

ABSTRACT

Changes of functional connectivity in prodromal and early Alzheimer's disease can arise from compensatory and/or pathological processes. We hypothesized that i) there is impairment of effective inhibition associated with early Alzheimer's disease that may lead to ii) a paradoxical increase of functional connectivity. To this end we analyzed effective connectivity in 14 patients and 16 matched controls using dynamic causal modeling of functional MRI time series recorded during a visual inter-hemispheric integration task. By contrasting co-linear with non co-linear bilateral gratings, we estimated inhibitory top-down effects within the visual areas. The anatomical areas constituting the functional network of interest were identified with categorical functional MRI contrasts (*Stimuli*>*Baseline* and *Co-linear gratings*>*Non co-linear gratings*), which implicated V1 and V3v in both hemispheres. A model with reciprocal excitatory intrinsic connections linking these four regions and modulatory inhibitory effects exerted by V3v on V1 optimally explained the functional MRI time series in both subject groups. However, Alzheimer's disease was associated with significantly weakened intrinsic and modulatory connections. Top-down inhibitory effects, previously detected as relative deactivations of V1 in young adults, were observed neither in our aged controls nor in patients. We conclude that effective inhibition weakens with age and more so in early Alzheimer's disease.

Introduction

Neuroimaging and morphological studies consistently show deterioration of cortico-cortical connections in Alzheimer's disease (AD) (Zhou et al., 2008; Stebbins and Murphy, 2009; Di Paola et al., 2010a, 2010b; Fornari et al., in press). However, measurements of resting-state functional connectivity based on the temporal correlations of fMRI or EEG time series reveal a more complex picture. Reductions and increases in coupling between areas may reflect combinations of decreases in long-range functional connections associated with increases in those at short-range (Horwitz et al., 1995; Wang et al., 2007). Reduced functional connectivity between left hippocampus and multiple cortical regions along with its increase to the right lateral prefrontal cortex described in mild AD patients is another example (L. Wang et al., 2006). Our recent EEG report also demonstrated an AD-specific connectivity landscape in the resting-state characterized by hypo-synchronization over prefrontal and hyper-synchronization over posterior regions including parietal, temporal, and occipital cortices (Knyazeva et al., 2010).

An increase of functional connectivity in early AD can be interpreted in different ways. The most accepted account suggests a compensatory response due to axonal sprouting and synaptic plasticity (Adams, 1991). An alternative interpretation is based on the observation that selective *coupling* of activity between the distributed cortical areas involved in a particular cognitive process is supplemented by selective *decoupling* of areas irrelevant to it (Rodriguez et al., 1999; Silberstein, 2006). If the capacity to attenuate irrelevant functional connections is impaired in AD, the result may be increased fMRI/EEG synchronization. Thus, both scenarios could lead to an increase of functional connectivity. Moreover, both could result in augmented activation and/or excessive recruitment of territories as documented by fMRI in prodromal or early AD (Becker et al., 1996; Grady et al., 2003; Morcom et al., 2003; Dickerson et al., 2005; Pariente et al., 2005; Sperling, 2007).

While indistinguishable with analysis of *functional* connectivity, the underlying processes will result in differential patterns of *effective* connectivity. Effective connectivity evaluates the influence that one local neural system (source) exerts on another (target) by a method such as dynamic causal modeling (DCM) (Friston et al., 2003). DCM differentiates positive coupling that results from correlated increased activity between a source and target region from negative coupling that results in a relative decrease in the target compared to the source, presumably from an attenuation of inputs from source to target. We therefore used DCM analyses to disambiguate network activity changes characteristic of early AD.

We chose to examine effective connectivity in a restricted neural network, using the visual inter-hemispheric integration task (IIT) (Knyazeva et al., 2006a; Knyazeva et al., 2006b). This task contrasts

* Corresponding author at: Department of Neurology, CHUV, 1011 Lausanne, Switzerland.
E-mail address: Maria.Knyazeva@chuv.ch (M.G. Knyazeva).

1053-8119/$ – see front matter © 2011 Elsevier Inc. All rights reserved.
doi:10.1016/j.neuroimage.2011.05.029

co-linear with orthogonal bilateral gratings, of which only the first generates a Gestalt such that the stimulus parts are fused between hemispheres. In agreement with predictive coding theory (Friston and Kiebel, 2009), more coherent stimuli should cause activations in higher-order and deactivations in lower-order visual areas. Indeed this phenomenon has been observed in various visual integration tasks (Murray et al., 2004; Knyazeva et al., 2006a). As recently shown with DCM, such dynamics depend on top-down and lateral inhibition and bottom-up excitation (Cardin et al., 2011). Therefore, we argued that the IIT would permit estimation of the strength of top-down inhibitory processes within the visual cortices.

We hypothesized that such inhibitory mechanisms are impaired in early AD and attempted, with DCM, to find supportive evidence of impaired intrinsic and/or context-sensitive modulations of effective visual connections in early AD patients compared to aged control subjects.

Methods

Patients and control subjects

This study is based on the functional MRI data of fourteen newly diagnosed AD patients from a larger sample in which the topography of functional cortical connectivity was studied with EEG (Knyazeva et al., 2010) and the topography of demyelination by Magnetization Transfer Imaging (Fornari et al., in press). The patients were recruited from the Memory Clinic of the Neurology Department (CHUV, Lausanne). The AD group included 14 patients (6 women and 8 men, Table 1). Sixteen control subjects (9 women and 7 men) were volunteers enrolled mostly from patients' partners, caregivers, or family members. The patient and control groups differed neither in age nor in level of education. All but one participant in each group was right-handed. All patients, caregivers, and control subjects gave written informed consent. All the applied procedures conform to the Declaration of Helsinki (1964) of the World Medical Association concerning human experimentation and were approved by the local Ethics Committee of Lausanne University.

The clinical diagnosis of probable AD was made according to the NINCDS-ADRDA criteria (McKhann et al., 1984), allowing a certainty of about 80–85% in the diagnosis. Cognitive functions were assessed with the Mini Mental State Examination (MMSE, (Folstein et al., 1975)) and with a detailed standardized neuropsychological assessment scale developed by the GRECO group for French speakers (Puel and Hugonot-Diener, 1996). To improve compatibility across studies, the stage of dementia was determined by the Clinical Dementia Rating Scale (CDR, (Morris, 1993)). For this study we selected patients with mild dementia (CDR 0.5–1). Complete laboratory analyses and diagnostic neuroimaging (CT or MRI) were performed in order to rule out cognitive dysfunction related to causes other than AD. Exclusion criteria comprised severe physical illness, psychiatric or neurological disorders associated with potential cognitive dysfunction, other dementia conditions (fronto-temporal dementia, dementia associated with Parkinsonism, Lewy body disease, pure vascular or prion dementia, etc.), alcohol/drug abuse, regular use of neuroleptics, antidepressants with anticholinergic action, benzodiazepines, stimulants, or β-blockers, and stages of AD beyond CDR 0.5–1.

Control subjects underwent a brief clinical interview and the MMSE to confirm the absence of cognitive deficits, of the use of psychoactive drugs, and of diseases that could interfere with cognitive function. Only individuals with no cognitive complaints and a score ≥ 28 for a high and ≥ 26 for a low level of education were accepted as controls. All control subjects underwent a brain MRI.

Table 1
Demographic and neuro-psychologic characteristics of AD patients and control subjects. The second and third columns present group characteristics, mean ± SD. The fourth column presents *P* values for the statistical significance of the between-group differences estimated by Mann–Whitney–Wilcoxon test. "W" stands for women, "M" for men.

Characteristic	Patients	Controls	*P*
Number of subjects	14	16	–
Gender	6 W / 8 M	9 W / 7 M	–
Age	68.4 ± 10.8	63.6 ± 11.9	0.40
Education	11.3 ± 3.4	13.3 ± 3.4	0.15
MMSE	21.3 ± 4.1	28.9 ± 1.1	0.001
Disease duration	4.2 ± 2.2	–	–
CDR	1.3 ± 0.6	–	-

Stimuli

The stimuli used for the IIT were bilateral iso-oriented co-linear and orthogonally oriented gratings centered on a fixation point (Fig. 1). *Co-linear gratings* (CG) consisted of two identical patches of co-linear, downward-drifting horizontal gratings on both sides of the fixation point. *Non co-linear* (*orthogonal) gratings* (NG) consisted of a patch of horizontal downward-drifting gratings on one side and a patch of vertical rightward-drifting gratings on the other. All gratings were of spatial frequency of 0.5 cycles per degree at a Michelson contrast of 70%; unilateral patches on a screen in the scanner measured 11.5 (width) by 19 deg (height). They drifted with a temporal frequency of 2 Hz. To compensate for retinal naso-temporal overlap and possible imperfect gaze fixation, all stimuli were separated from the vertical meridian of the visual field by a narrow stripe of background equal to 1 deg on each side. A uniform grey screen of same space-averaged luminance as the stimuli (32 cd/sqm) with a fixation point in the center served as *a baseline condition*. Importantly, this IIT paradigm requires limited subject compliance-steady visual fixation. It was monitored by an MR-compatible eye-tracking system (SMI, Germany) in several randomly chosen subjects (for details see (Knyazeva et al., 2006b)). In all patients and controls with recordings there was stable fixation within a circle of diameter of 2 deg centered on the fixation point for at least 95% of the stimulation time across all experimental conditions.

fMRI protocol

The fMRI experiment followed a block design paradigm, where 15 s of moving gratings alternated with 15 s of baseline grey screen. Both CG and NG stimuli were presented 6 times in a balanced-randomized order with an LCD projector at a refresh rate of 75 Hz. The projector was equipped with a photographic zoom lens projecting images onto a translucent screen in a custom-made mirror box, designed to minimize light reflections. It allowed a subject to view stimuli within a space defined by 25 deg horizontally and 19 deg vertically.

Functional MRI images were acquired on a Philips 3T Achieva scanner with an EPI gradient echo T2*-weighted sequence (FA 90, TE 30, matrix size 128×128, FoV 256, 16 slices, 5 mm thick, acquisition time 1.1 s) with a TR = 3 s. fMRI pre-processing steps, performed with SPM8 (Wellcome Department of Cognitive Neurology, London, UK), included realignment of intra-session acquisitions to correct for head movement, normalization to a standard template (Montreal Neurological Institute (MNI) template) to minimize inter-subject morphological variability and convolution with an isotropic Gaussian kernel (FWHM = 9 mm) to increase signal to noise ratio. Single subject analysis was performed according to the General Linear Model. The signal drift across acquisitions was removed with a high-pass filter.

Group statistics for SPM

Statistical parametrical maps of the contrasts of interest were computed for each subject as input values for the group statistics

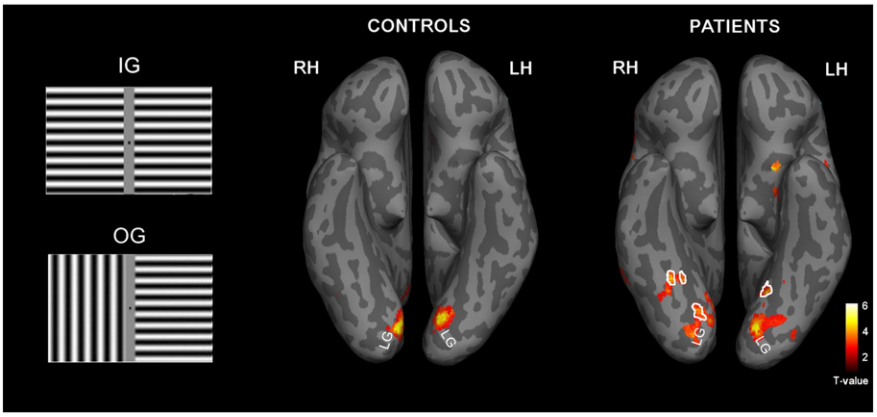

Fig. 1. The inter-hemispheric integration effects as revealed by the fMRI activation. Statistical maps of the *CG>NG* contrast for the control and AD groups are superimposed on inflated brains (bottom view). BOLD increase within and around the lingual gyrus is evident in both groups, but it is more extensive in the patients (both maps were thresholded at $P<0.005$). The centers of the clusters are 10, −80, −6 (right) and −16, −78, −10 (left) for the controls, and 10, −80, −12 (right) and −10, −82, -12 (left) for the AD patients (Talairach coordinates). Hot scale represents *T* values. The territories, where signal intensity is significantly higher in patients than in controls, are outlined in the patients' image. The sulci are presented in dark gray and the gyri in light gray. Anatomical labels: CoS, collateral sulcus; FG, fusiform gyrus; LG, lingual gyrus. LH stands for the left hemisphere, RH, for the right hemisphere.

based on Random Field Theory. Clusters with a height threshold set at $P<0.005$ (*t*-test) and extent threshold $k>30$ contiguous voxels in the group SPMs were used to identify the nodes of our model. Further, cluster local maxima were used as centers of Regions of Interest (ROI) for DCM analysis.

Dynamic causal modeling

DCM considers the brain as a dynamic system, in which external inputs cause changes in neuronal activity which, in turn, cause changes in the resulting distributed fMRI signals (Friston et al., 2003). Thus, DCM serves to infer the architecture of distributed brain networks based on recorded fMRI time series. The basic idea is to model interactions between neural sources such that the predicted regional BOLD signals that result from converting the modeled neural dynamics into hemodynamic responses will give the optimal balance between goodness-of-fit and model complexity. Mathematically DCMs for fMRI include a bilinear model for neuro-dynamics and an extended balloon model for hemodynamics (Buxton et al., 1998; Friston et al., 2003). Since the theoretical and practical issues of DCM were recently reviewed, we refer interested readers to these sources for more details of the method and underlying theory (Seghier et al., 2010; Stephan and Friston, 2010).

Optimal model selection

The neuro-dynamic model depends on the experimental manipulation. Thus, brain regions included in the model, anatomical connections between them, driving and modulatory inputs all have to be specified. Such a specification includes the definition of a relevant model space, given prior knowledge about the system. We used a Bayesian model selection procedure to choose the optimal model. The aim of this step was to achieve an optimal compromise between model accuracy and complexity (Stephan et al., 2009). To this end, we used negative variational free-energy, an approximation of log-evidence, as a measure of model goodness. First, we calculated the free-energy estimations for each subject and competing model; second, we pooled them across subjects for each model and further used them for model comparison. The model with largest log-evidence was considered the best. The exponential of differences between the free energies for any two models was interpreted as weak (1–3), positive (3–20), strong (20–150), or very strong (≥ 150) evidence for preferring one model over another (Raftery, 1995; Penny et al., 2004). DCM was performed using SPM8 software.

Group statistics for DCM

For statistical inference at a group level we used the framework of random-effects analysis (Stephan et al., 2009). To test for differences between models and to explore the effects of AD on coupling parameters for the best model, an analysis of variance (ANOVA) was used. The planned comparisons were performed, when necessary, by means of two-sampled two-sided *t*-tests. The connectivity parameters of the best model were characterized descriptively by one-sampled two-sided *t*-tests. Significant effects are reported at $P<0.05$ corrected for multiple comparisons. All statistical tests were implemented with SPSS 17.0 for Windows.

Results

Both stimulus conditions were associated with extensive activation of striate and extra-striate areas in patients and controls. We determined individual anatomical locations of activation maxima in a step-wise fashion guided by activated regions in conjunction maps of categorical CG and NG contrasts (further referred to as the *Stimulus>Baseline* contrast). Firstly we concentrated on areas within or close to the primary visual cortex. Attribution of anatomical labels was done with the help of a probabilistic cytoarchitectonic atlas (Eickhoff et al., 2005). Activations were thus identified in both experimental groups, mainly in Brodmann area 17 (Table 2). Then, examining simple effects between stimuli, we found that in the *CG>NG* contrast (Fig. 1) there were bilateral extra-striate BOLD increases centered on the lingual gyri (V3v) in both controls and patients. The mean distances between the two maxima were 16.33 and 14.79 mm in the left hemisphere and 13.27 and 16.23 mm in the right for controls and patients, respectively. The absence of significant

Table 2
Anatomical location and cluster size of regions activated by gratings. Coordinates of the centers of activated clusters are given according to Talairach and Tournoux (1988). Cluster sizes for the *CG≥NG* contrast are in brackets.

Group	CG>Baseline		CG>NG	
	Hemisphere			
	Left	Right	Left	Right
Controls	75% V1/25%V2	63% V1/37%V2	78%V3v/22%V2 (443)	41%V3v/59%V2 (202)
Patients	66% V1/34%V2	72% V1/28%V2	71%V3v/29%V2 (478)	52%V3v/48%V2 (254)

overlap is provided by the fact that each of these distances is larger than the side of a resolution element (one resel contains 101 voxel of size $2\times2\times2$ mm^3, which is equivalent to a volume of $9.3\times9.3\times9.3$ mm^3) in this fMRI study (Worsley et al., 1996). The activated territory was larger in patients than in controls, especially in the right lingual gyrus (for cluster size see Table 2). A direct comparison within the region of interest, restricted to clusters activated in patients, revealed a statistically significant between-group difference in signal intensity (patients>controls) at $P<0.05$ in territories not activated in controls in the contrast *CG>Baseline* (outlined in Fig. 1). In the *NG>CG* contrast there were no significant BOLD activations ($P>0.5$).

Consequently, we included two pairs of ROIs in our model, further referred to as $V1_L$, $V1_R$, $V3_L$, and $V3_R$. The ROIs in individual subjects (Supplementary Table S1) were localized as the local maxima nearest to respective group maxima. For each subject the original 120-scan time series were extracted as the first principal component of all voxel time series within a sphere of 4 mm radius centered on the individual local maxima. Two subjects (a control and a patient) were excluded from the DCM because no activations were found in them.

Definition of intrinsic, modulatory, and driving connections

First, we selected a model with optimal intrinsic connections, applying a Bayesian approach to the set of models with probable connectivity structure (Fig. 2). In all competing models the *Stimulus>Baseline* contrast served as the driving input. We modeled the presentation of bilateral gratings and crossed visual pathways by allowing the right and left visual field stimuli to directly affect the left and right primary visual cortices respectively. The induced activity then spread through the system as a function of the model-defined intrinsic connections.

Since the number of all possible four-area models with four possible states for each connection (reciprocal or two unidirectional or no connection) is 4096, we had to reduce the model-space to a feasible number. To determine the most probable pattern of effective connectivity between $V1_L$, $V1_R$, $V3_L$, and $V3_R$, we considered evidence from human studies and from animal models credibly extendable to humans (Van Essen et al., 1982; Innocenti, 1986; Olivares et al., 2001; Clarke, 2003). The first model (A1) includes well-established reciprocal intra-hemispheric connections between V1 and V3 and homotopic inter-hemispheric connections via the corpus callosum (CC) at both levels of the visual hierarchy. Similar models have been used in previous DCM studies (Stephan et al., 2007).

However, callosal connections between primary visual areas are sparse and restricted to a narrow stripe along the border between V1 and V2. Their function may be limited in adult human brain. These observations motivated us to include a second model, lacking such connections (B1). In addition to classical homotopic inter-hemispheric connections, there exist heterotopic visual inter-hemispheric connections (Segraves and Innocenti, 1985), which may be significant for human cognitive functions (Clarke, 2003). To take these into account, we added models C1 and D1. It is noteworthy, that previously published models have ignored this type of connections (Stephan et al., 2007).

The pathological process in AD affects cortico-cortical connections relatively early, including those crossing the CC (Di Paola et al., 2010b) and intra-hemispheric association fibers (Fornari et al., in press). The detailed topography and mechanisms of their degeneration are unknown. Yet converging evidence suggests that the association areas suffer much earlier than primary areas. Therefore, we assumed that inter-hemispheric and bottom-up connections from primary visual areas are relatively spared in early AD. Also, we considered the possibility of asymmetric effects in early AD (Grady et al., 1986; Haxby

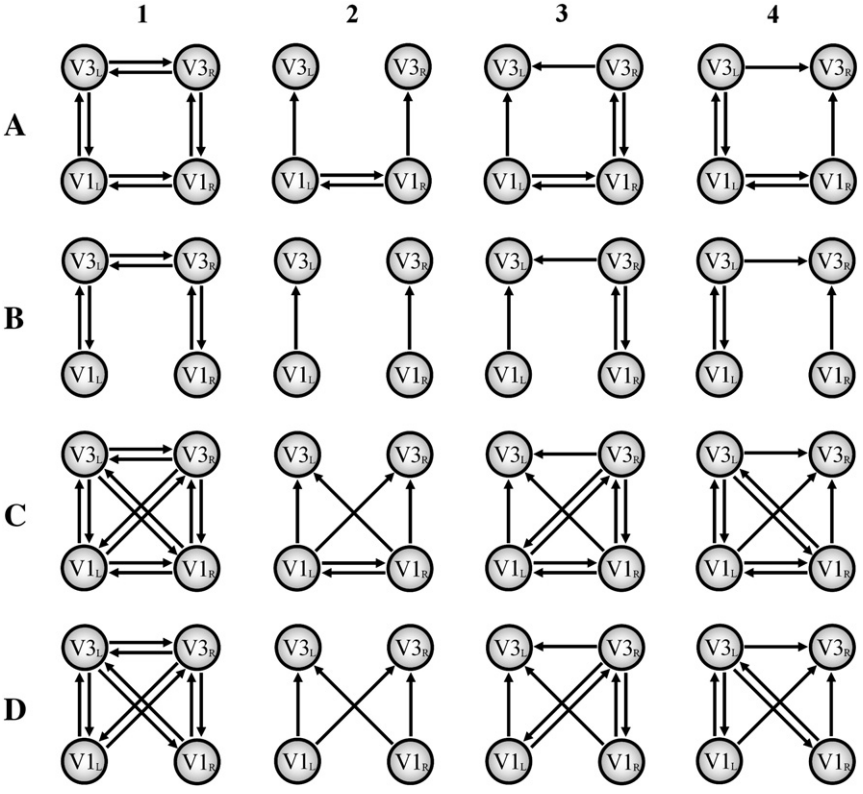

Fig. 2. Competing DCMs of effective connectivity. Gray filled circles symbolize the brain regions involved in the modeled network. They are located in the left and right primary visual cortex ($V1_L$ and $V1_R$, respectively) and in the left and right V3v ($V3_R$ and $V3_L$, respectively). Arrows between the circles stand for the bidirectional intrinsic connections. For simplicity, the driving inputs provided by the bilateral gratings (Fig. 1) directly to $V1_L$ (the right visual field stimulus) and to $V1_R$ (the left visual field stimulus) independently of a model are omitted. For further details see Results, where each model is designated by a capital letter and a number, which stand for its column and row, respectively.

et al., 1990; Boxer et al., 2003; Chaim et al., 2007; Li et al., 2008; Jacobson et al., 2009). The resulting set of models included symmetrically (A2, B2, C2, D2) and asymmetrically (8 models in columns 3 and 4) broken connections from V3 in both left and right hemispheres.

We then considered probable modulatory effects superimposed on the optimal intrinsic connection model (Fig. 3). Since inter-hemispheric integration induced by a Gestalt generating stimulus can be a source of modulatory effects, we modeled the difference between CG and NG conditions. To account for such effects within extra-striate visual areas (Knyazeva et al., 2006a; Knyazeva et al., 2006b; Fang et al., 2008), we added homotopic inter-hemispheric modulatory connections between V3 regions (model M1). Recent findings of modulatory effects on early visual areas (Murray et al., 2004; Ban et al., 2006; Fang et al., 2008; Cardin et al., 2011) are reflected in models M2-M4. Finally, modulatory influences on extra-striate areas can originate from the primary visual areas and be conveyed via intra-hemispheric and heterotopic inter-hemispheric pathways as suggested by model M5. The simplest of these (M1–M2) specify only inter- or intra-hemispheric modulatory effects, while models M3–M5 include both types of modulation. Such modulation can be implemented *via* purely homotopic inter-hemispheric pathways (M3) or through heterotopic and homotopic backward (M4) and additional forward (M5) inter-hemispheric pathways.

Effective connectivity in AD and normal aging

The model with reciprocal heterotopic and homotopic connections C1 generated the best connectivity structure within the chosen set of models (Fig. 2; Table S2). The log-evidences pooled across subjects for each model indicated strong evidence in favor of C1 over the second best model in both groups. To test the differences in log-evidence over models and subject groups, a two-way repeated-measures ANOVA was performed. The Group factor had 2 levels (controls vs. AD patients) and the Model factor had 16 levels (the log evidences for 16 competing models). This test revealed a significant effect of the Model factor ($P<0.0001$, $F=31.976$, $df=2.073$, Greenhouse–Geisser corrected) with a large effect size ($\eta^2=0.552$). The *planned* *t*-test comparisons showed significant differences between the optimal (C1) and second best models for controls (C3, $P<0.0001$) and patients (C4, $P=0.002$). The main effect of Group was also significant ($P=0.008$, $F=8.283$, $df=1$; $\eta^2=0.242$) with log evidences for patients lesser than those of controls (Table S2).

Once the connectivity structure was defined, we focused on how this intrinsic coupling is modulated by the experimental conditions, i.e., by inter-hemispheric integration. To this end, we superimposed plausible models M1–M5 of modulatory effects on the best model of intrinsic connections C1. According to the log-evidences summed across subjects, M4 was found to be optimal for controls and patients, with strong evidence over the second best model M5 for controls and patients (Table S3). To confirm this finding we performed a two-way ANOVA with Model (log evidences for the five competing models) and Group (controls vs. patients) factors. The Model factor appeared significant ($P<0.0001$, $F=96.01$, $df=1.33$, Greenhouse–Geisser corrected) with a large effect size ($\eta^2=0.787$). The *planned* *t*-test comparisons validated significant differences between the optimal model M4 and second best model M5 for controls ($P<0.0001$) and patients ($P=0.00011$). The main effect of Group failed to reach significance ($P=0.062$).

Group-averaged estimates of the strength of intrinsic connections for the optimal model are summarized in Fig. 4A (Table S4). All parameters significantly differed from zero ($P=0.05$, two-sided Bonferroni corrected *t*-tests). To explore the effects of AD on the strength of intrinsic connections and interactions of this pathology with the topography of connections, we performed a three-way mixed between-within ANOVA with Group (controls vs. AD patients), Hemisphere (connections from the left hemisphere ($L\rightarrow R$), vs. connections from the right hemisphere ($L\leftarrow R$)), and Topography (4 levels: $V1_L\leftrightarrow V1_R$, $V3_L\leftrightarrow V3_R$, $V1\rightarrow V3$, and $V1\leftarrow V3$ connections) factors. The main effect of Group was significant ($P=0.014$, $F=6.9$, $df=1$) with a large effect size ($\eta^2=0.21$). As seen in Fig. 4B, the strength of intrinsic connections was strongly reduced in the AD group. This effect of AD significantly interacted with Hemisphere and Topography factors ($P=0.039$, $F=4.19$, $df=1.35$, Greenhouse–Geisser corrected; $\eta^2=0.139$). The *planned* (between-group) comparisons showed significantly weaker inter-hemispheric connections of the left primary visual area in patients ($V1_L\rightarrow V1_R$ at $P=0.045$ and $V1_L\rightarrow V3_R$ at $P=0.01$).

All but one ($V3_L\rightarrow V3_R$ in controls) modulatory connection significantly differed from zero ($P<0.05$, two-sided Bonferroni corrected *t*-tests). Their group-averaged strength estimates (Fig. 5A; Tables S4) were analyzed with a three-way ANOVA that included the Group and Hemisphere factors as described in the previous paragraph, and a Topography factor (3 levels: intra-hemispheric $V3\rightarrow V1$; inter-hemispheric $V3_L\leftrightarrow V3_R$, and $V3\rightarrow V1$ connections). Although there was no main effect of Group, there was a significant interaction with Hemisphere ($P=0.027$, $F=5.525$, $df=1$, Greenhouse–Geisser corrected; $\eta^2=0.175$). As Fig. 5B shows, strong modulations with the right hemisphere were weakened in AD, but not the weak modulations originating from the left hemisphere.

The direct effects of visual gratings on V1 were significant but weak (Supplementary Tables S4C, S5C). The estimates of driving inputs were analyzed by means of a 2-way mixed between-within ANOVA with Group (controls vs. patients) and Hemisphere (driving input to left vs. right hemisphere) factors. The only significant effect was weaker driving inputs in the AD than the control group ($P=0.005$, $F=9.569$, $df=1$; $\eta^2=0.269$) (Fig. 6).

Discussion

Plastic brain changes in response to a pathological process can be analyzed in terms of system reorganization through transformation of its elements and/or connectivity (Will et al., 2008). To reveal what happens with inhibitory coupling at an early stage of AD before "remodeling," we limited our analysis to the visual network that seemed to have similar elements in aged controls and mild AD patients. In the context of AD studies, the visual cortex is of particular interest, as it is relatively mildly affected at an early stage of the

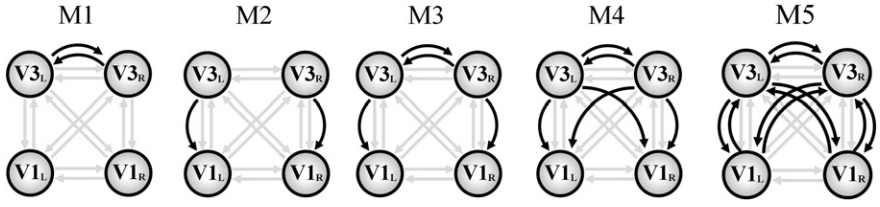

Fig. 3. Competing dynamic causal models with modulatory effects. These DCMs are based on the optimal model C1 chosen among the models of intrinsic connectivity from Fig. 2 and designated here with gray arrows. Modulatory inputs are shown with black arrows. Other designations are as in Fig. 2. The models differ in that they either specify only inter- or intra-hemispheric (M1-M2) or both types (M3-M5) of modulatory effects.

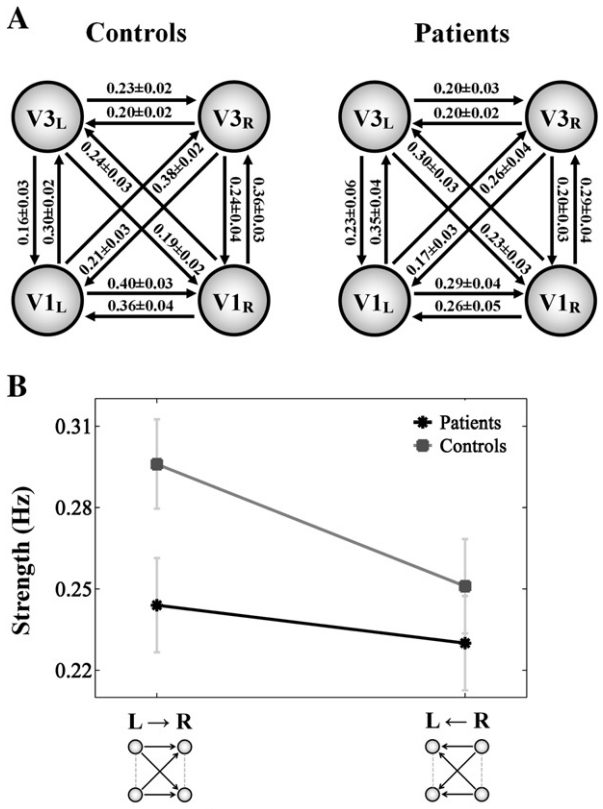

Fig. 4. Intrinsic connections for the optimal model in control and patient groups. A: The average estimates of the strength of intrinsic connections in Hertz with standard errors are shown alongside the respective connections. Other designations are as in Fig. 2. B: The main effect of AD on the strength of intrinsic connections. The means and standard errors of the strength of intrinsic connections are presented. See Results for details.

disease, making detection of compensatory changes more feasible. Indeed, in response to the IIT, the system demonstrated some attributes characteristic of responses thought to be compensatory, e.g., relative over-recruitment in extra-striate areas (Fig. 1).

Our analysis capitalized on recent findings that coherent and/or meaningful stimuli cause activations in higher-order and deactivations in lower-order visual areas involved in their processing (Murray et al., 2004; Knyazeva et al., 2006a; Knyazeva et al., 2006b). This dynamic is explained by predictive coding theory as a manifestation of a hierarchical optimization mechanism based on feedback connections that carry predictions of lower-level neural activity and feedforward connections that carry residual errors between predictions and actual lower-level responses (Rao and Ballard, 1999; Friston and Kiebel, 2009). Top-down and lateral effects are thought to be inhibitory and bottom-up effects excitatory (Cardin et al., 2011). To evaluate the strength of inhibitory processes, we contrasted bilateral co-linear gratings (Gestalt) and bilateral orthogonal gratings (no Gestalt), of which only the first stimulus can be inter-hemispherically integrated. In agreement with the predictive coding theory, we anticipated that co-linear stimuli would cause relative activations in the extra-striate and deactivations in the striate visual areas.

Indeed, in both groups, the contrast *CG>NG*, presumably reflecting the processes of inter-hemispheric integration, resulted in bilateral extra-striate BOLD activations in the lingual gyrus (Fig. 1), mainly corresponding to area V3v (Table 2). Previously, we observed similar extra-striate responses to the same stimuli in young adults (Knyazeva et al., 2006a,b) and in children (Fornari et al., 2007). At the same time, the contrast *NG>CG* failed to reveal relative deactivation of the primary visual cortex in either group. Task-related deactivations in early visual areas have previously been shown only in young adults. Furthermore, aged controls and AD patients have impaired deactivations in the "default mode network" when engaged in active tasks (Lustig et al., 2003; Sperling, 2007; Frings et al., 2010). Our DCM analysis suggests that, at least in AD patients, this effect can be explained by a weakening of inhibitory feedback connections (Fig. 5).

Before discussing this central issue, we summarize the main facts obtained in our experiments. Both control and patient fMRI time series are best explained by the same DCM, in which reciprocal homotopic and heterotopic intrinsic connections link four regions located symmetrically in V3v and V1 visual areas. At the same time, AD clearly affected the strength of intrinsic connections and the effects of driving inputs. All significantly changed connections were attenuated in patients, especially in the left hemisphere (Fig. 4). This weakening of context-independent (built-in) effective connections is in good agreement with neuro-anatomical and neuroimaging data about changes in cortico-cortical connectivity of the visual brain in AD, which are best exemplified by plentiful CC studies.

The fibers that form the splenium of the CC implement interhemispheric interaction in the ventral visual stream (Gazzaniga, 2000; Dougherty et al., 2005; Zarei et al., 2006). Poorly myelinated fibers of small diameter are abundant in this region (Aboitiz et al., 1992). Such fibers are among the last to myelinate and the first to be damaged by age-related changes and AD (Bartzokis, 2004). As a result, the splenial area diminishes with age, and these changes are more pronounced in AD (Pantel et al., 1999; Yamauchi et al., 2000; Teipel et al., 2003; P.J. Wang et al., 2006). The impaired integrity of splenium fibers in AD patients has been also documented by diffusion tensor/weighted imaging studies (Medina et al., 2006; Chua et al., 2008;

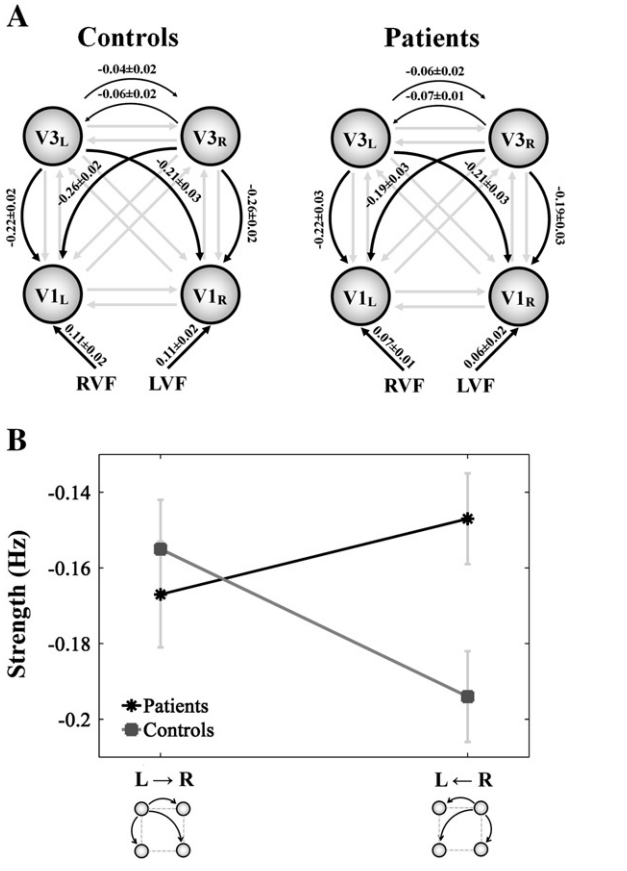

Fig. 5. Modulatory connections for the optimal model in control and patient groups. A: The average estimates of modulatory parameters in Hertz with standard errors are shown alongside the respective connections. Other designations are as in Fig. 2. B: The effects of AD on the strength of modulatory connections from the left and right hemispheres. The means and standard errors of the strength of modulatory connections are presented. See Results for details.

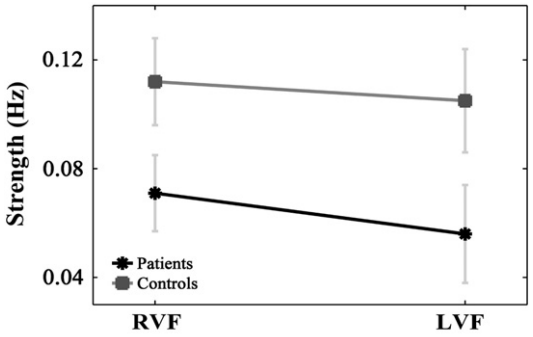

Fig. 6. Main effect of AD on driving input. The means and standard errors of the strength of driving inputs from the right visual field (RVF) and left visual field (LVF) in control and patient groups are presented. See Results for details.

Parente et al., 2008; Ukmar et al., 2008; Di Paola et al., 2010a, 2010b). However, these changes are very weak in mild AD and major only at a late stage of the disease (Hensel et al., 2002; Di Paola et al., 2010b). In contrast, with DCM analysis, we were readily able to detect the changes in effective connectivity (Figs. 4–5) that we associate with early AD.

As expected, intrinsic connections were modulated by the IIT both in controls and in AD patients. Moreover, all modulatory effects, including top-down and lateral, were found to be inhibitory. Noteworthily, the lateral extra-striate effects were weaker than top-down effects, including the heterotopic inter-hemispheric inputs. Since DCM does not imply any assumptions about the number of synapses implementing a connection, it remains to be demonstrated whether the heterotopic callosal connections shown in animals and humans (Segraves and Innocenti, 1985; Clarke, 2003) are involved in these mechanisms.

Therefore, our evidence supports previous findings of negative backward coupling associated with visual processing at higher-order levels of the visual hierarchy (Cardin et al., 2011). In all probability, deactivations induced by visual integration tasks in the primary visual cortex (Murray et al., 2004; Fang et al., 2008) are also based on the trans-callosal or intra-hemispheric inhibition rather than on purely hemodynamic mechanisms. This inference is supported by the independence of the hemispheric blood supplies in the case of deactivation of cortex ipsilateral to a stimulated hemi-field (Brandt et al., 2000; Shmuel et al., 2003) and by callosum-mediated modulatory effects shown in animals (Schmidt et al., 2010).

Thus, we have an apparent inconsistency in our data between the inhibitory effects shown in a network analysis and their absence in simple task-dependent contrasts. This may be a result of age-related degradation of effective connectivity or of greater sensitivity of the DCM method, which looks for context-dependent changes specifically. The latter interpretation is further supported by the significant differences found between AD patients and controls that also fail to reach significance in simple contrasts of state-dependent activity. Specifically, in AD patients, the strength of top-down modulations from right V3 was reduced in the right hemisphere, where we also observed the most pronounced over-recruitment effects (Figs. 1, 5B). We suggest that this asymmetry is task rather than AD associated because of the evidence that similar perceptual tasks involve the right more than the left hemisphere (e.g., Knyazeva et al. 2010b) and because our controls have stronger modulatory connections in the right hemisphere with the IIT.

Overall, our results imply that functional deactivations normally occurring in the early visual areas in young adults (Murray et al., 2004; Ban et al., 2006; Fang et al., 2008; Cardin et al., 2011) that are presumably based on the inhibitory effects of modulatory top-down connections are reduced in the aged population and even more so in early AD. Impaired deactivations in the elderly are not limited to the default mode network as previously shown (Lustig et al., 2003; Sperling, 2007; Frings et al., 2010), but are more distributed and probably have a common cause—attenuation or loss of functional inhibition. These findings allow a reconciliation of conflicting reports about impaired anatomical integrity and increasing functional connectivity, as the anatomical changes lead to an attenuation of functional inhibition. Since functional inhibition is a necessary element of distributed brain network interactions, these changes appear to be maladaptive. It remains to be confirmed whether our findings can be generalized to brain networks other than the visual. Episodic memory and subtending hippocampal connectivity networks are complex cognitive functions ripe for further study in AD patients using this technique.

Given these phenomena such as altered effective connectivity, functional over-recruitment of cortical areas, etc. are among the features of early AD, it is possible they may constitute exploitable candidate biomarkers of developing AD even in a prodromal stage. Further in-depth investigations are therefore warranted. Of special interest is that deactivations of the primary visual areas were absent not only in AD patients, but also in aged controls (Table S1), suggesting an age-sensitive nature of this phenomenon. Evaluation of network inhibition may be especially useful for preclinical identification of prodromal AD if the results of these group studies can be translated to an individual level.

Supplementary materials related to this article can be found online at doi:10.1016/j.neuroimage.2011.05.029.

Acknowledgments

This work was supported by Swiss National Foundation grant #320030-127538/1. It was also supported by the Centre d'Imagerie BioMédicale (CIBM) of the University of Lausanne (UNIL), the Swiss Federal Institute of Technology Lausanne (EPFL), the University of Geneva (UniGe), the Centre Hospitalier Universitaire Vaudois (CHUV), the Hôpitaux Universitaires de Genève (HUG) and the Leenaards and the Jeantet Foundations.

We thank G. Batistella for his assistance in processing neuroimaging data and Dr. F. Kherif for helpful discussions and insightful comments. We also thank the two anonymous reviewers for their constructive comments and recommendations.

References

Aboitiz, F., Scheibel, A.B., Fisher, R.S., Zaidel, E., 1992. Fiber composition of the human corpus callosum. Brain Res. 598, 143–153.
Adams, I.M., 1991. Structural plasticity of synapses in Alzheimer's disease. Mol. Neurobiol. 5 (2–4), 411–419.
Ban, H., Yamamoto, H., Fukunaga, M., Nakagoshi, A., Umeda, M., Tanaka, C., et al., 2006. Toward a common circle: interhemispheric contextual modulation in human early visual areas. J. Neurosci. 26 (34), 8804–8809.
Bartzokis, G., 2004. Age-related myelin breakdown: a developmental model of cognitive decline and Alzheimer's disease. Neurobiol. Aging 25 (1), 5–18 author reply 49–62..
Becker, J.T., Mintun, M.A., Aleva, K., Wiseman, M.B., Nichols, T., DeKosky, S.T., 1996. Compensatory reallocation of brain resources supporting verbal episodic memory in Alzheimer's disease. Neurology 46 (3), 692–700.
Boxer, A.L., Kramer, J.H., Du, A.T., Schuff, N., Weiner, M.W., Miller, B.L., et al., 2003. Focal right inferotemporal atrophy in AD with disproportionate visual constructive impairment. Neurology 61 (11), 1485–1491.
Brandt, T., Stephan, T., Bense, S., Yousry, T.A., Dieterich, M., 2000. Hemifield visual motion stimulation: an example of interhemispheric crosstalk. Neuroreport 11 (12), 2803–2809.
Buxton, R.B., Wong, E.C., Frank, L.R., 1998. Dynamics of blood flow and oxygenation changes during brain activation: the balloon model. Magn. Reson. Med. 39 (6), 855–864.
Cardin, V., Friston, K.J., Zeki, S., 2011. Top-down modulations in the visual form pathway revealed with dynamic causal modeling. Cereb. Cortex 21 (3), 550–562.
Chaim, T.M., Duran, F.L., Uchida, R.R., Perico, C.A., de Castro, C.C., Busatto, G.F., 2007. Volumetric reduction of the corpus callosum in Alzheimer's disease in vivo as assessed with voxel-based morphometry. Psychiatry Res. 154 (1), 59–68.

Chua, T.C., Wen, W., Slavin, M.J., Sachdev, P.S., 2008. Diffusion tensor imaging in mild cognitive impairment and Alzheimer's disease: a review. Curr. Opin. Neurol. 21 (1), 83–92.
Clarke, S., 2003. The role of homotopic and heterotopic callosal connections in man. In: Zaidel, E., Iacoboni, M. (Eds.), The parallel brain: the cognitive neuroscience of the corpus callosum. MIT Press, Cambridge: MA, pp. 461–472.
Di Paola, M., Luders, E., Di Iulio, F., Cherubini, A., Passafiume, D., Thompson, P.M., et al., 2010a. Callosal atrophy in mild cognitive impairment and Alzheimer's disease: different effects in different stages. Neuroimage 49 (1), 141–149.
Di Paola, M., Spalletta, G., Caltagirone, C., 2010b. In vivo structural neuroanatomy of corpus callosum in Alzheimer's disease and mild cognitive impairment using different MRI techniques: a review. J. Alzheimers Dis. 20 (1), 67–95.
Dickerson, B.C., Salat, D.H., Greve, D.N., Chua, E.F., Rand-Giovannetti, E., Rentz, D.M., et al., 2005. Increased hippocampal activation in mild cognitive impairment compared to normal aging and AD. Neurology 65 (3), 404–411.
Dougherty, R.F., Ben-Shachar, M., Bammer, R., Brewer, A.A., Wandell, B.A., 2005. Functional organization of human occipital-callosal fiber tracts. Proc Natl Acad Sci USA 102 (20), 7350–7355.
Eickhoff, S.B., Stephan, K.E., Mohlberg, H., Grefkes, C., Fink, G.R., Amunts, K., et al., 2005. A new SPM toolbox for combining probabilistic cytoarchitectonic maps and functional imaging data. Neuroimage 25 (4), 1325–1335.
Fang, F., Kersten, D., Murray, S.O., 2008. Perceptual grouping and inverse fMRI activity patterns in human visual cortex. J. Vis. 8 (7), 21–29.
Folstein, M.F., Folstein, S.E., McHugh, P.R., 1975. "Mini-mental state." A practical method for grading the cognitive state of patients for the clinician. J. Psychiatr. Res. 12, 189–198.
Fornari, E., Knyazeva, M.G., Meuli, R., Maeder, P., 2007. Myelination shapes functional activity in the developing brain. Neuroimage 38 (3), 511–518.
Fornari, E., Maeder, P., Meuli, R., Ghika, J., Knyazeva, M.G., in press. Demyelination of superficial white matter in early Alzheimer's disease: a magnetization transfer imaging study. Neurobiol. Aging. doi:10.1016/j.neurobiolaging.2010.11.014.
Frings, L., Dressel, K., Abel, S., Saur, D., Kummerer, D., Mader, I., et al., 2010. Reduced precuneus deactivation during object naming in patients with mild cognitive impairment, Alzheimer's disease, and frontotemporal lobar degeneration. Dement. Geriatr. Cogn. Disord. 30 (4), 334–343.
Friston, K., Kiebel, S., 2009. Predictive coding under the free-energy principle. Philos. Trans. R. Soc. Lond. B Biol. Sci. 364 (1521), 1211–1221.
Friston, K.J., Harrison, L., Penny, W., 2003. Dynamic causal modelling. Neuroimage 19 (4), 1273–1302.
Gazzaniga, M.S., 2000. Cerebral specialization and interhemispheric communication: does the corpus callosum enable the human condition? Brain 123 (Pt 7), 1293–1326.
Grady, C.L., Haxby, J.V., Schlageter, N.L., Berg, G., Rapoport, S.I., 1986. Stability of metabolic and neuropsychological asymmetries in dementia of the Alzheimer type. Neurology 36 (10), 1390–1392.
Grady, C.L., McIntosh, A.R., Beig, S., Keightley, M.L., Burian, H., Black, S.E., 2003. Evidence from functional neuroimaging of a compensatory prefrontal network in Alzheimer's disease. J. Neurosci. 23 (3), 986–993.
Haxby, J.V., Grady, C.L., Koss, E., Horwitz, B., Heston, L., Schapiro, M., et al., 1990. Longitudinal study of cerebral metabolic asymmetries and associated neuropsychological patterns in early dementia of the Alzheimer type. Arch. Neurol. 47 (7), 753–760.
Hensel, A., Wolf, H., Kruggel, F., Riedel-Heller, S.G., Nikolaus, C., Arendt, T., et al., 2002. Morphometry of the corpus callosum in patients with questionable and mild dementia. J. Neurol. Neurosurg. Psychiatry 73 (1), 59–61.
Horwitz, B., McIntosh, A.R., Haxby, J.V., Furey, M., Salerno, J.A., Schapiro, M.B., et al., 1995. Network analysis of PET-mapped visual pathways in Alzheimer type dementia. Neuroreport 6 (17), 2287–2292.
Innocenti, G.M., 1986. General organization of callosal connections in the cerebral cortex. In: Jones, E.G., Peters, A. (Eds.), Cerebral Cortex. Plenum Publishing Corporation, New York, pp. 291–353.
Jacobson, M.W., McEvoy, L.K., Dale, A., Fennema-Notestine, C., 2009. Cognitive phenotypes, brain morphometry and the detection of cognitive decline in preclinical AD. Behav. Neurol. 21 (1), 29–37.
Knyazeva, M.G., Fornari, E., Meuli, R., Innocenti, G., Maeder, P., 2006a. Imaging of a synchronous neuronal assembly in the human visual brain. Neuroimage 29 (2), 593–604.
Knyazeva, M.G., Fornari, E., Meuli, R., Maeder, P., 2006b. Interhemispheric integration at different spatial scales: the evidence from EEG coherence and FMRI. J. Neurophysiol. 96 (1), 259–275.
Knyazeva, M.G., Jalili, M., Brioschi, A., Bourquin, I., Fornari, E., Hasler, M., et al., 2010. Topography of EEG multivariate phase synchronization in early Alzheimer's disease. Neurobiol. Aging 31 (7), 1132–1144.
Li, S., Pu, F., Shi, F., Xie, S., Wang, Y., Jiang, T., 2008. Regional white matter decreases in Alzheimer's disease using optimized voxel-based morphometry. Acta Radiol. 49 (1), 84–90.
Lustig, C., Snyder, A.Z., Bhakta, M., O'Brien, K.C., McAvoy, M., Raichle, M.E., et al., 2003. Functional deactivations: change with age and dementia of the Alzheimer type. Proc. Natl. Acad. Sci. U.S.A. 100 (24), 14504–14509.
McKhann, G., Drachman, D., Folstein, M., Katzman, R., Price, D., Stadlan, E.M., 1984. Clinical diagnosis of Alzheimer's disease: report of the NINCDS-ADRDA Work Group under the auspices of Department of Health and Human Services Task Force on Alzheimer's Disease. Neurology 34 (7), 939–944.
Medina, D., DeToledo-Morrell, L., Urresta, F., Gabrieli, J.D., Moseley, M., Fleischman, D., et al., 2006. White matter changes in mild cognitive impairment and AD: a diffusion tensor imaging study. Neurobiol. Aging 27 (5), 663–672.
Morcom, A.M., Good, C.D., Frackowiak, R.S., Rugg, M.D., 2003. Age effects on the neural correlates of successful memory encoding. Brain 126 (Pt 1), 213–229.
Morris, J.C., 1993. The clinical dementia rating (CDR): current version and scoring rules. Neurology 43, 2412–2414.
Murray, S.O., Schrater, P., Kersten, D., 2004. Perceptual grouping and the interactions between visual cortical areas. Neural Netw. 17 (5–6), 695–705.
Olivares, R., Montiel, J., Aboitiz, F., 2001. Species differences and similarities in the fine structure of the mammalian corpus callosum. Brain Behav. Evol. 57 (2), 98–105.
Pantel, J., Schroder, J., Jauss, M., Essig, M., Minakaran, R., Schonknecht, P., et al., 1999. Topography of callosal atrophy reflects distribution of regional cerebral volume reduction in Alzheimer's disease. Psychiatry Res. 90 (3), 181–192.
Parente, D.B., Gasparetto, E.L., da Cruz, L.C., Domingues Jr., R.C., Baptista, A.C., Carvalho, A.C., 2008. Potential role of diffusion tensor MRI in the differential diagnosis of mild cognitive impairment and Alzheimer's disease. AJR Am. J. Roentgenol. 190 (5), 1369–1374.
Pariente, J., Cole, S., Henson, R., Clare, L., Kennedy, A., Rossor, M., et al., 2005. Alzheimer's patients engage an alternative network during a memory task. Ann. Neurol. 58 (6), 870–879.
Penny, W.D., Stephan, K.E., Mechelli, A., Friston, K.J., 2004. Comparing dynamic causal models. Neuroimage 22 (3), 1157–1172.
Puel, M, Hugonot-Diener. Presenting by the GRECO group of the French adaptation of a cognitive assessment scale used in Alzhiemer type dementia. 25. 1996;22(22): 1028–1032.
Raftery, A.E., 1995. Bayesian model selection in social research. Sociological Methodology. 25, 111–196.
Rao, R.P., Ballard, D.H., 1999. Predictive coding in the visual cortex: a functional interpretation of some extra-classical receptive-field effects. Nat. Neurosci. 2 (1), 79–87.
Rodriguez, E., George, N., Lachaux, J.P., Martinerie, J., Renault, B., Varela, F.J., 1999. Perception's shadow: long-distance synchronization of human brain activity. Nature 397 (6718), 430–433.
Schmidt, K.E., Lomber, S.G., Innocenti, G.M., 2010. Specificity of neuronal responses in primary visual cortex is modulated by interhemispheric corticocortical input. Cereb. Cortex 20 (12), 2776–2786.
Seghier, M.L., Zeidman, P., Neufeld, N.H., Leff, A.P., Price, C.J., 2010. Identifying abnormal connectivity in patients using dynamic causal modeling of FMRI responses. Front Syst Neurosci. 4.
Segraves, M.A., Innocenti, G.M., 1985. Comparison of the distributions of ipsilaterally and contralaterally projecting corticocortical neurons in cat visual cortex using two fluorescent tracers. J. Neurosci. 5 (8), 2107–2118.
Shmuel, A., Augath, M., Rounis, E., Logothetis, N.K., Smirnakis, S., 2003. Negative BOLD response ipsilateral to the visual stimulation: origin is not blood stealing. Neuroimage 19 (2), S309 (Supplement 1).
Silberstein, R.B., 2006. Dynamic sculpting of brain functional connectivity and mental rotation aptitude. Prog. Brain Res. 159, 63–76.
Sperling, R., 2007. Functional MRI studies of associative encoding in normal aging, mild cognitive impairment, and Alzheimer's disease. Ann. N. Y. Acad. Sci. 1097, 146–155.
Stebbins, G.T., Murphy, C.M., 2009. Diffusion tensor imaging in Alzheimer's disease and mild cognitive impairment. Behav. Neurol. 21 (1), 39–49.
Stephan, K.E., Friston, K.J., 2010. Analyzing effective connectivity with functional magnetic resonance imaging. Wiley Interdisciplinary Reviews. Cognitive Science. 1 (3), 446–459.
Stephan, K.E., Marshall, J.C., Penny, W.D., Friston, K.J., Fink, G.R., 2007. Interhemispheric integration of visual processing during task-driven lateralization. J. Neurosci. 27 (13), 3512–3522.
Stephan, K.E., Penny, W.D., Daunizeau, J., Moran, R.J., Friston, K.J., 2009. Bayesian model selection for group studies. Neuroimage 46 (4), 1004–1017.
Teipel, S.J., Bayer, W., Alexander, G.E., Bokde, A.L., Zebuhr, Y., Teichberg, D., et al., 2003. Regional pattern of hippocampus and corpus callosum atrophy in Alzheimer's disease in relation to dementia severity: evidence for early neocortical degeneration. Neurobiol. Aging 24 (1), 85–94.
Ukmar, M., Makuc, E., Onor, M.L., Garbin, G., Trevisiol, M., Cova, M.A., 2008. Evaluation of white matter damage in patients with Alzheimer's disease and in patients with mild cognitive impairment by using diffusion tensor imaging. Radiol. Med. 113 (6), 915–922.
Van Essen, D.C., Newsome, W.T., Bixby, J.L., 1982. The pattern of interhemispheric connections and its relationship to extrastriate visual areas in the macaque monkey. J. Neurosci. 2 (3), 265–283.
Wang, L., Zang, Y., He, Y., Liang, M., Zhang, X., Tian, L., et al., 2006. Changes in hippocampal connectivity in the early stages of Alzheimer's disease: evidence from resting state fMRI. Neuroimage 31 (2), 496–504.
Wang, P.J., Saykin, A.J., Flashman, L.A., Wishart, H.A., Rabin, L.A., Santulli, R.B., et al., 2006. Regionally specific atrophy of the corpus callosum in AD, MCI and cognitive complaints. Neurobiol. Aging 27 (11), 1613–1617.
Wang, K., Liang, M., Wang, L., Tian, L., Zhang, X., Li, K., et al., 2007. Altered functional connectivity in early Alzheimer's disease: a resting-state fMRI study. Hum. Brain Mapp. 28 (10), 967–978.
Will, B., Dalrymple-Alford, J., Wolff, M., Cassel, J.C., 2008. The concept of brain plasticity —Paillard's systemic analysis and emphasis on structure and function (followed by the translation of a seminal paper by Paillard on plasticity). Behav. Brain Res. 192 (1), 2–7.

Worsley, K.J., Marrett, S., Neelin, P., Vandal, A.C., Friston, K.J., Evans, A.C., 1996. A unified statistical approach for determining significant signals in images of cerebral activation. Hum. Brain Mapp. 4 (1), 58–73.

Yamauchi, H., Fukuyama, H., Nagahama, Y., Katsumi, Y., Hayashi, T., Oyanagi, C., et al., 2000. Comparison of the pattern of atrophy of the corpus callosum in frontotemporal dementia, progressive supranuclear palsy, and Alzheimer's disease. J. Neurol. Neurosurg. Psychiatry 69 (5), 623–629.

Zarei, M., Johansen-Berg, H., Smith, S., Ciccarelli, O., Thompson, A.J., Matthews, P.M., 2006. Functional anatomy of interhemispheric cortical connections in the human brain. J. Anat. 209 (3), 311–320.

Zhou, Y., Dougherty, J.H., Hubner, K.F., Bai, B., Cannon, R.L., Hutson, R.K., 2008. Abnormal connectivity in the posterior cingulate and hippocampus in early Alzheimer's disease and mild cognitive impairment. Alzheimers Dement. 4 (4), 265–270.